Leukodystrophy resembling Vanishing White Matter Disease is recapitulated by brain-specific depletion of apoptosis regulator MCL-1

Running title: MCL-1 is required for white matter integrity

Abigail H. Cleveland[1,2], Alejandra Romero[3], Laurent Alfonso Azcona[2], Melisa Herrero[4], Orna Elroy-Stein[4,5], Vivian Gama[3,6,7] and Timothy R. Gershon[2,8,9]

[1]UNC Cancer Cell Biology Training Program, University of North Carolina, Chapel Hill, North Carolina 27599, USA

[2]Department of Neurology, UNC School of Medicine, University of North Carolina, Chapel Hill, North Carolina 27599, USA

[3]Vanderbilt University, Cell and Developmental Biology, Nashville, Tennessee 37232, USA .

[4]Shmunis School of Biomedicine and Cancer Research, Faculty of Life Sciences, Tel Aviv University, Tel Aviv, Israel

[5]Sagol School of Neuroscience, Tel Aviv University, Tel Aviv, Israel

[6]Vanderbilt University, Vanderbilt Center for Stem Cell Biology, Nashville, Tennessee 37232, USA .

[7]Vanderbilt University, Vanderbilt Brain Institute, Nashville, Tennessee 37232, USA .

[8]UNC Neuroscience Center, University of North Carolina, Chapel Hill, North Carolina 27599, USA

[9]Lineberger Comprehensive Cancer Center, University of North Carolina, Chapel Hill, North Carolina 27599, USA

Co-corresponding authors: Vivian Gama (vivian.gama@vanderbilt.edu) and Timothy R. Gershon (gershont@neurology.med.unc.edu)

Acknowledgments: supported by R01NS088219 (TRG), R01NS102627 (TRG), and R01NS1062 (TRG), T32CA071341 (AHG), 4R00CA178190 (VG), R35GM128915 (VG), and R21CA227483 (VG).

SUMMARY

Diverse mutations cause leukodystrophies through unresolved processes. Developing leukodystrophy therapies requires identifying mechanisms that operate downstream of causative mutations to produce white matter degeneration. We have identified the apoptosis regulator MCL-1 as required for white matter stability and depleted by leukodystrophy-causing mutations. Brain-specific deletion of *Mcl-1* in mice recapitulates progressive leukodystrophy, with MRI changes, decreased oligodendrocytes, and astrocytic and microglial changes typical of Vanishing White Matter Disease (VWMD). Disabling apoptosis through co-deletion of *Bax* or *Bak* rescued white matter *Mcl-1*-dependence, broadly implicating the intrinsic apoptotic pathway in leukodystrophy pathogenesis. *Bax* and *Bak* co-deletions rescued different aspects of the *Mcl-1*-deleted phenotype, demonstrating their discrete roles in white matter stability. MCL-1 protein abundance was reduced in *eif2b5*-mutant mice that model VWMD, suggesting a mechanistic relationship between MCL-1 and VWMD. Our data show that oligodendrocytes require MCL-1 to suppress apoptosis, implicate MCL-1 loss in VWMD pathogenesis, and suggest inhibiting apoptosis for leukodystrophy therapy.

Introduction

Leukodystrophies are a heterogeneous group of severe neurodegenerative disorders marked by progressive white matter disruption [1,2]. The age of onset varies in each leukodystrophy, but patients typically become symptomatic during childhood, after a latent, asymptomatic period [3,4]. Patients with leukodystrophies may experience progressive symptoms including ataxia, dementia, hallucinations, seizures, coma,

60 and death [5]. There is currently no specific targeted therapy that has been clinically
61 implemented to arrest the progression of any leukodystrophy.

62 Diverse pathogenic mutations have been linked to different leukodystrophies
63 [6], but the mechanistic processes through which specific mutations cause white matter
64 degeneration are incompletely understood. Mutations in the apoptotic regulator
65 *APOPT1* (aka *COA8*) cause Progressive Cavitating Leukoencephalopathy,
66 suggesting a role for inappropriate apoptosis in this disease [7,8]. However, it is not
67 clear why this mutation specifically affects cells of the white matter. Mutations in
68 *eIF2B* subunits result in Vanishing White Matter Disease (VWMD), another
69 leukodystrophy similarly marked by white matter cavitation [9-11]. The causative role of
70 *eIF2B* mutations implicates impaired mRNA translational regulation in VWMD
71 pathogenesis, associated with activation of the Integrated Stress Response (ISR) [12-
72 17]. Prior studies have not identified a role for apoptosis in VWMD causation, as seen
73 in Progressive Cavitating Leukoencephalopathy, and whether a common pathogenic
74 process unites these similar phenotypes is unclear.

75 Studies in *eIf2b5* $^{R132H/R132H}$ mice provide insight into the disproportionate effect
76 of *eIF2B* mutations on white matter. These mice develop leukodystrophy resembling
77 VWMD and show impaired mitochondrial function in fibroblasts, astrocytes, and
78 oligodendrocytes [18-20]. These studies suggest that *eIF2B* mutations disproportionately
79 affect white matter because glia are more dependent than other types cells on
80 accurate translational regulation and mitochondrial function [21]. However, several
81 unresolved steps are required to connect the biological processes that have been
82 found to be disrupted in Progressive Cavitating Leukoencephalopathy and VWMD to
83 the observed disease process of progressive leukodystrophy.

84 Identifying proteins that are both required for white matter integrity and
85 affected by *eIF2B* mutations may show specific mechanisms that link VWMD
86 genotype and phenotype. Defining these mechanistic links may show why diverse
87 leukodystrophy mutations produce the final common pathology of white matter
88 degeneration. Identifying proximal mediators of white matter degeneration may also
89 provide important insight into leukodystrophy pathogenesis and treatment.

90 Here we report that mice with conditional deletion of the anti-apoptotic
91 regulator *Mcl-1* targeted to brain stem cells develop progressive postnatal white
92 matter degeneration that recapitulates the phenotype of human leukodystrophies,
93 particularly VWMD. MCL-1 promotes the survival of different cell lineages through its
94 ability to inhibit the pro-apoptotic proteins BAK and BAX, the main effectors of cell
95 death in mammalian cells. Importantly, MCL-1 is a mitochondrial protein that is
96 translationally suppressed by ISR activity [22], while VWMD disrupts mitochondria and
97 activates the ISR, raising the possibility the MCL-1 deficiency could play a role in the
98 VWMD phenotype.

99 *Mcl-1*-deleted mice were born with normal brain anatomy and show normal
100 motor control and behavior at postnatal day 7 (P7), but then develop increasingly
101 severe ataxia, abnormal motor responses, and extensive white matter atrophy. This
102 white matter-predominant neurodegenerative process closely matches the course of
103 human leukodystrophies with similar postnatal onset of symptoms, MRI changes,
104 progressive white matter degeneration, reduced oligodendrocyte populations,
105 astrocytic abnormalities, and microglial accumulation. Mutations that block the
106 intrinsic apoptotic pathway rescued the phenotype of *Mcl-1* deletion, implicating
107 apoptosis in leukodystrophy pathogenesis, and suggesting a potential approach to
108 therapy.

109

110

111 **Results**

112 **Conditional *Mcl-1* deletion in the CNS causes progressive white matter**
113 **degeneration.**

114 We generated mice with conditional, brain-specific *Mcl-1* deletion by breeding
115 *Mcl-1*$^{loxP/loxP}$ mice that harbor loxP sites around exon 1 of the *Mcl1* locus [23], with
116 *GFAP-Cre* mice that express Cre recombinase in stem cells that give rise to the
117 neurons and glia of the cerebrum and cerebellum, excluding the Purkinje cells (Supp
118 fig. 1A-B) [24,25]. The resulting *hGFAP-Cre/Mcl-1*$^{loxP/loxP}$ (*Mcl-1*^{cKO}) mice were born at
119 the expected Mendelian ratio.

120 We compared *Mcl-1*^{cKO} mice to littermate controls, including *Mcl-1*$^{loxP/loxP}$ mice
121 without Cre and heterozygously deleted *hGFAP-Cre/Mcl-1*$^{loxP/+}$. We found no
122 differences between control genotypes and therefore pooled them for analysis.
123 During the first week of life, *Mcl-1*^{cKO} mice showed no deficits and gained weight
124 similarly to controls (Fig. 1A). However, by P14, *Mcl-1*^{cKO} mice showed reduced
125 weight gain (Fig. 1A) and progressive neurologic impairment. While control mice
126 showed normal ability to be weaned at P21, *Mcl-1*^{cKO} mice were unable to be weaned
127 and all died by P23.

128 *Mcl-1*^{cKO} mice demonstrated progressive abnormalities of motor function. We
129 used developmentally adjusted tests to compare behavior of *Mcl-1*^{cKO} mice and
130 controls at P7, P14, and P18. To examine behavior at P7, when mice do not yet have
131 open eyes and do not venture from the nest, we used a test of geotaxis by placing

132 mice on a tilted screen and measuring latency to turn. We also measured latency to
133 turn over in a righting test, and we counted pivots during a 3-min open field test. We
134 found no genotype-specific differences at P7 (Table 1).

135

Test	WT	*Mcl-1*^{cKO}
Negative geotaxis (latency, s)		
Trial 1	15.4 ± 2	14.3 ± 3
Trial 2	15.1 ± 2	16.7 ± 3
Trial 3	15.3 ± 2	20.9 ± 3
Righting (latency, s)	8.2 ± 1	10.0 ± 3
Number of pivots	1.7 ± 0.3	1.3 ± 0.5

136

137 **Table 1. Neonatal behavior testing showed no effects of *Mcl-1*^{cKO} genotype**
138 **at P7.** Each test was performed on 48 replicate WT pups and 13 replicate *Mcl-*
139 *1*^{cKO} pups at P7. Measures included latency to turn on a tilted screen in a test for
140 geotaxis, and latency to turn over in a righting test. Pivots were counted by an
141 experimenter during a 3-min open field test. One-way ANOVA found no
142 statistically significant differences.

143

144 In contrast to the similar behaviors at P7, by P14 *Mcl-1*^{cKO} mice showed
145 decreased rearing when placed in an open field and spent more time in the center of
146 the open field, while traveling similar distances compared to controls (Fig. 1B; Supp
147 fig. 1C). P18 *Mcl-1*^{cKO} mice also showed a marked increase in limb clasping when
148 vertically suspended (Fig. 1C), a commonly used marker of disease progression in a
149 number of mouse models of neurodegeneration and ataxia [26,27].

150 Responses to sensory input were abnormal in *Mcl-1*^{cKO} mice and changed over
151 time. At P14, mice showed increased amplitude of acoustic startle response (Fig. 1D).
152 By P21, when motor function was significantly impaired, the amplitude of acoustic
153 startle response was markedly diminished compared to controls. These data show
154 reduced inhibition in response to sensory stimuli at P14, and reduced motor
155 responses at later ages.

156 Neuropathology studies demonstrated progressive white matter degeneration,
157 that began after the first week of life. At P7, *Mcl-1*^{cKO} brains showed no abnormalities
158 and appeared similar to controls. At P14, *Mcl-1*^{cKO} mice showed white matter
159 rarefaction and ventricular dilation and these changes were more pronounced at P21
160 (Fig. 1E). In addition to white matter loss, we also noted migration abnormalities in
161 the cerebellum, with ectopic cerebellar granule cells in the molecular layer of the
162 cerebellum (Fig. 1E). *Mcl-1*^{cKO} thus showed progressive neuropathology that
163 corresponded temporally with the onset of neurologic symptoms, beginning after P7
164 and increasing over time.

165

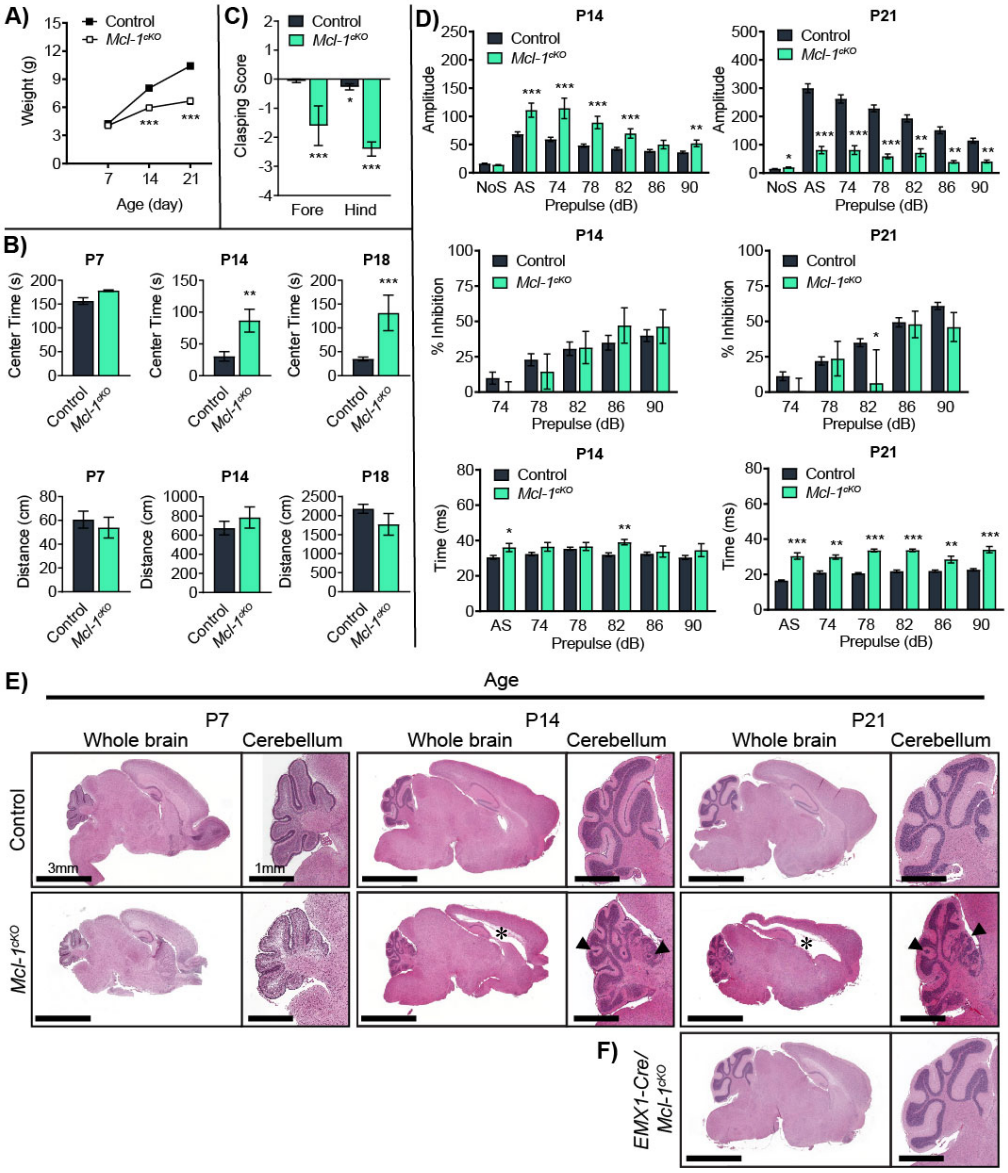

166

167 **Figure 1. *Mcl-1* deletion causes progressive motor impairment and white matter**
168 **degeneration.** (**A**) Reduced weight gain in *Mcl-1*^{cKO} mice compared to controls. (**B**)
169 *Mcl-1*^{cKO} mice show normal motor function at P7, with altered motor function by P14
170 and (**C**) increased hind-limb clasping at P18. (**D**) *Mcl-1*^{cKO} mice show increased startle
171 in response to auditory stimuli at P14, and reduced elicited movement at P21. (**E**)
172 Brains of representative *Mcl-1*^{cKO} mice shown in H&E-stained sagittal sections appear
173 similar to controls at P7. By P14, *Mcl-1*^{cKO} mice develop white matter degeneration
174 with ventricular enalargment (*) and abnormal migration of cerebellar granule neurons
175 (arrows). White matter loss increases by P21. (**F**) Deleting *Mcl-1* in the neuron-

176 specific *Emx* lineage in *EMX1-Cre/Mcl-1*$^{loxP/loxP}$ mice does not recapitulate the *Mcl-*
177 *1*^{cKO} phenotype. *, ** and *** denote p<0.05, p<0.01 and p<0.001 respectively, relative
178 to controls.

179 ***Mcl-1* deletion must occur in glia to cause white matter degeneration.**

180 The *GFAP-Cre* transgenic line induces recombination in a broad lineage that
181 includes both glia and neurons [24]. In order to determine whether *Mcl-1* loss in neurons
182 drives the *Mcl-1*^{cKO} phenotype, we deleted *Mcl-1* with the neuron-specific *EMX1-Cre*
183 by crossing *Mcl-1*$^{loxP/loxP}$ and *EMX1-Cre* mouse lines. The resulting *EMX1-Cre/Mcl-*
184 *1*$^{loxP/loxP}$ mice did not develop white matter degeneration or ventriculomegaly (Fig. 1F).
185 In contrast, deletion of *Mcl-1* in *Nestin-Cre/Mcl-1*$^{loxP/loxP}$ mice produced white matter
186 degeneration as seen in *Mcl-1*^{cKO} mice (Supp Fig. 2). *Nestin-Cre*, like *GFAP-Cre*,
187 drives recombination in stem cells with neural and glial potential. The phenotype of
188 white matter degeneration thus required *Mcl-1* deletion in the glial lineage.

189 **Blocking apoptosis prevents white matter degeneration in *Mcl-1*-deleted mice**

190 To determine if white matter degeneration in *Mcl-1*^{cKO} mice resulted from
191 increased apoptosis, we examined cell death through cleaved caspase-3
192 immunohistochemistry and TUNEL assays. We did not detect an increase in cleaved
193 caspase-3-stained cells at P7, prior to the onset of white matter loss, or at P14, after
194 white matter loss was evident (data not shown). However, TUNEL staining, performed
195 at P11 when white matter loss was developing, demonstrated increased cell death in
196 *Mcl-1*^{cKO} brains, consistent with a pro-apoptotic effect of *Mcl-1* deletion (Fig. 2A).

197 To determine whether the increased cell death in *Mcl-1*-deleted mice was
198 causally related to the white matter degeneration, we tested whether blocking
199 apoptosis through co-deletion of either *Bax* or *Bak* rescued the *Mcl-1*^{cKO} phenotype.

200 We repeatedly intercrossed *Mcl-1*^{cKO} mice with *Bax*$^{loxP/LoxP}$/*Bak*$^{-/-}$ mice to generate
201 animals with conditional deletion of *Mcl-1* and heterozygous or homozygous deletion
202 of *Bax* or *Bak*. We then raised pups of each genotype and analyzed survival,
203 neurologic function, and neuropathology.

204 We found that co-deletion of *Bax* or *Bak* significantly suppressed the *Mcl-1*^{cKO}
205 phenotype, but resulted in different, mitigated phenotypes. *Mcl-1*-deleted mice with
206 heterozygous co-deletion of *Bak*, with the genotype *hGFAP-Cre/Mcl1*$^{loxP/loxP}$/*Bak*$^{-/+}$
207 (*Mcl-1*^{cKO}/*Bak*$^{-/+}$), showed normal survival without overt neurologic deficits and normal
208 white matter and cerebellar migration (Fig. 2B). In contrast, *Mcl-1*-deleted mice with
209 heterozygous co-deletion of *Bax*, with the genotype *hGFAP-Cre/Mcl1*$^{loxP/loxP}$/*Bax*$^{loxP/+}$
210 (*Mcl-1*^{cKO}/*Bax*$^{fl/+}$), showed a progressive leukoencephalopathy phenotype similar *Mcl-*
211 *1*^{cKO} mice (Fig. 2B). Immunohistochemistry demonstrated markedly lower BAK
212 protein in *Bak*$^{+/-}$ animals (Fig. 2C), indicating that that heterozygous *Bak* deletion was
213 sufficient to alter BAK expression. The rescued phenotype of *Mcl-1*^{cKO}/*Bak*$^{-/+}$ mice
214 therefore demonstrated reducing BAK protein expression was sufficient to prevent
215 white matter degeneration.

216

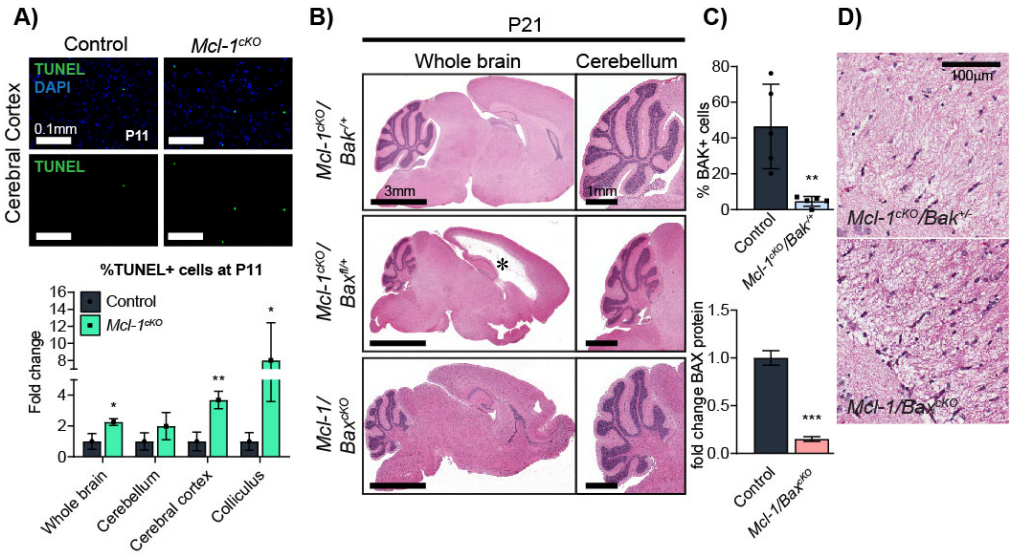

Figure 2. *Mcl-1* deletion causes white matter degeneration by increasing apoptosis. (**A**) TUNEL demonstrates increased cell death in *Mcl-1*^{cKO} brains. For cell counts, one sagittal section from each replicate was scanned at 20x and TUNEL+ cells were counted across the entire portion of each designated region that was contained within the section. (**B**) Representative H&E sections show that heterozygous *Bak* co-deletion and homozygous *Bax* co-deletion both rescue the white matter loss with ventricular enlargement (*) and cerebellar abnormalities caused by *Mcl-1* deletion. (**C**) Quantification of BAK immunohistochemistry in corpus callosum shows that heterozygous *Bak* deletion significantly reduces the number of BAK+ cells. Quantification of western blot of whole cerebella shows that homozygous *Bax* deletion reduces BAX protein abundance. (**D**) Representative images of the corpus callosum in P14 mice of the indicated genotypes shows mild white matter rarefaction in *Mcl-1/Bax*^{dKO} mice, not seen in *Mcl-1*^{cKO}*/Bak*$^{+/-}$ mice. *, ** and *** denote $p<0.05$, $p<0.01$ and $p<0.001$ respectively, relative to controls.

Mcl-1-deleted mice with homozygous *Bax* co-deletion, with the genotype *hGFAP-Cre/Mcl1*$^{loxP/loxP}$*/Bax*$^{loxP/loxP}$ (*Mcl-1/Bax*^{dKO}) showed normal survival, similar to *Mcl-1*^{cKO}*/Bak*$^{-/+}$ mice. Compared to *Mcl-1*^{cKO} mice, *Mcl-1/Bax*^{dKO} mice showed greatly reduced neurologic deficits; however, we noted that by 200 days, *Mcl-1/Bax*^{dKO} showed a slight delay in movement on opening the cage that was not seen in *Mcl-*

237 *1^{cKO}/Bak$^{+/-}$* mice. The extensive white matter loss in *Mcl-1^{cKO}* mice was rescued in
238 *Mcl-1/Bax^{dKO}* mice (Fig. 2B). Close examination of brain sections from *Mcl-1/Bax^{dKO}*
239 mice, however, showed mild white matter loss (Fig 2D). The rescued phenotypes of
240 *Mcl-1^{cKO}/Bak$^{-/+}$* and *Mcl-1/Bax^{dKO}* mice show that disrupting either *Bax* or *Bak* is
241 sufficient to prevent the severe white matter degeneration that otherwise results from
242 *Mcl-1* deletion, implicating apoptosis in the pathogenesis of the *Mcl-1^{cKO}* phenotype.
243 The mild neurologic deficits and white matter loss in *Mcl-1/Bax^{dKO}* mice showed that
244 co-deletion of *Bax* and *Bak* do not have identical effects in *Mcl-1*-deleted animals.

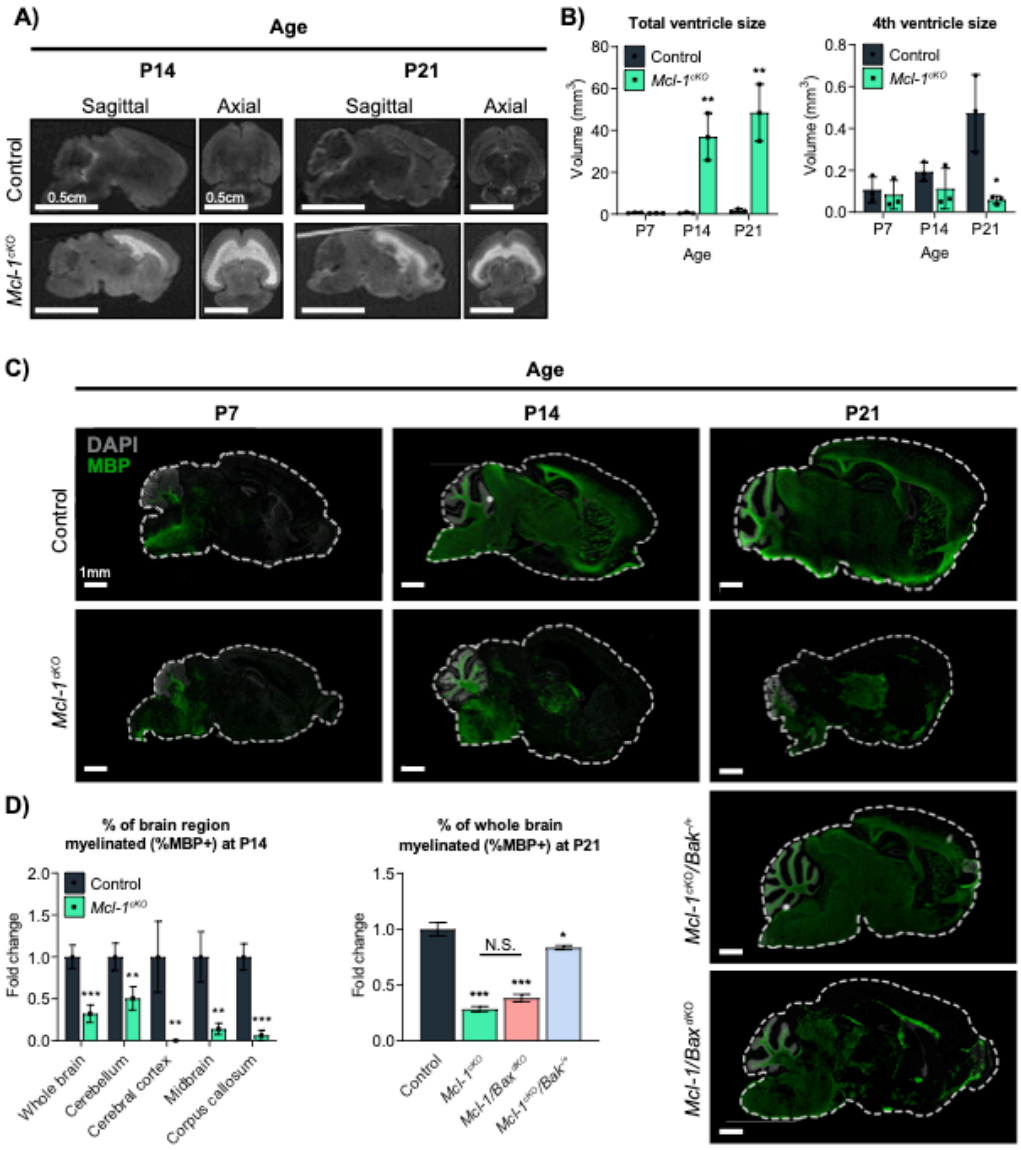

245

246 **Figure 3. Abnormal neuroimaging and myelination in *Mcl-1*-deleted mice, with**
247 **different rescue effects caused by co-deletion of *Bak* or *Bax*.** (**A**) Representative
248 MRIs show white matter hyperintensity in *Mcl-1*^{cKO} mice. (**B**) Total ventricular volume
249 is abnormal in *Mcl-1*^{cKO} mice and increases from P7-P21, while the volume of the 4th
250 ventricle decreases significantly by P21. (**C,D**) Representative images and
251 quantitative analysis of MBP IHC show that myelination is markedly decreased in *Mcl-*
252 *1*^{cKO} mice, rescued in *Mcl-1*^{cKO}*/Bak*$^{+/-}$ mice, and incompletely rescued in *Mcl-1/Bax*^{dKO}

253 mice. **(D)** Graphs show MBP+ area/total area within individual sections, normalized
254 to the mean value in the control mice. *, ** and *** denote $p<0.05$, $p<0.01$ and
255 $p<0.001$ respectively, relative to controls.

256 **Mcl-1 deletion phenocopies human leukodystrophies**

257 Leukoencephalopathies in patients produce characteristic MRI findings,
258 including high water signal in white matter tracts [5], and the replacement of white
259 matter by cerebrospinal fluid [11]. We analyzed whether *Mcl-1*^{cKO} mice showed similar
260 white matter changes on MRI. Similar to VWMD patients, *Mcl-1*^{cKO} mice showed
261 progressive ventriculomegaly (Fig. 3A). The increase in ventricle size was not evenly
262 distributed, however, as the volume of the 4th ventricle was significantly smaller in
263 *Mcl-1*^{cKO} mice at P21 (Fig. 3B). Increased lateral ventricles and reduced 4th ventricle
264 was consistent with loss of periventricular cerebral white matter and an overall
265 reduction in intracranial pressure, indicating hydrocephalus *ex vacuo*.

266 To determine whether myelination was disrupted in *Mcl-1*^{cKO} mice, we
267 analyzed the distribution of Myelin Basic Protein (MBP). In control brains, the MBP+
268 area increased markedly from P7 to P14 (Fig 3C). In contrast, myelination was
269 delayed in *Mcl-1*^{cKO} brains, which showed significantly less MBP+ area at P14 in all
270 brain regions analyzed (Fig. 3D).

271 Analysis of MBP+ area in *Mcl-1*-deleted mice with *Bax* or *Bak* co-deletions
272 showed that myelination required MCL-1 specifically to regulate BAK. We compared
273 brains in P21 animals, when normal brains show widespread myelination.
274 Heterozygous *Bak* co-deletion largely rescued myelination in *Mcl-1*^{cKO}/*Bak*$^{+/-}$ mice. In
275 these animals, MBP+ area was over 2-fold greater than in *Mcl-1*^{cKO} mice, although
276 we noted a small, statistically significant decrease in myelination compared to *Mcl-1*

277 intact controls. Homozygous *Bax* deletion, however, did not rescue myelination in
278 *Mcl-1/Bax*^{dKO} mice (Fig. 3D). The differential effects of *Bak* or *Bax* deletion on
279 myelination support the interpretation that BAX and BAK act in cells with different
280 functions, with both BAX and BAK affecting white matter maintenance, and only BAK
281 affecting myelination.

282

283 ***Mcl-1* deletion reduces oligodendrocyte and Bergmann glia populations**

284 To determine if impaired myelination in *Mcl-1*^{cKO} mice resulted from
285 oligodendrocyte loss, we compared the numbers of cells expressing the
286 oligodendrocyte marker SOX10 in *Mcl-1*^{cKO} and control mice (Fig. 4A). SOX10 marks
287 the oligodendrocyte lineage from the initial fate commitment in oligodendrocyte
288 precursors to the maturation of myelinating oligodendrocytes [31,32]; SOX10 cell counts
289 thus reflect the total oligodendrocytic population across the differentiation spectrum.
290 At P7, oligodendrocyte populations in *Mcl-1*^{cKO} mice were not significantly different
291 from controls. By P14, *Mcl-1*^{cKO} mice showed significantly fewer SOX10+ cells in
292 diverse brain regions (Fig. 4B), indicating a global decrease in oligodendrocytic cells.
293 At P21, oligodendrocytic populations remained reduced in the cerebellum, corpus
294 callosum, and superior colliculus, but were not statistically significantly reduced in the
295 hippocampus and cerebral cortex, raising the possibility of a dynamic, homeostatic
296 response in these gray matter regions.

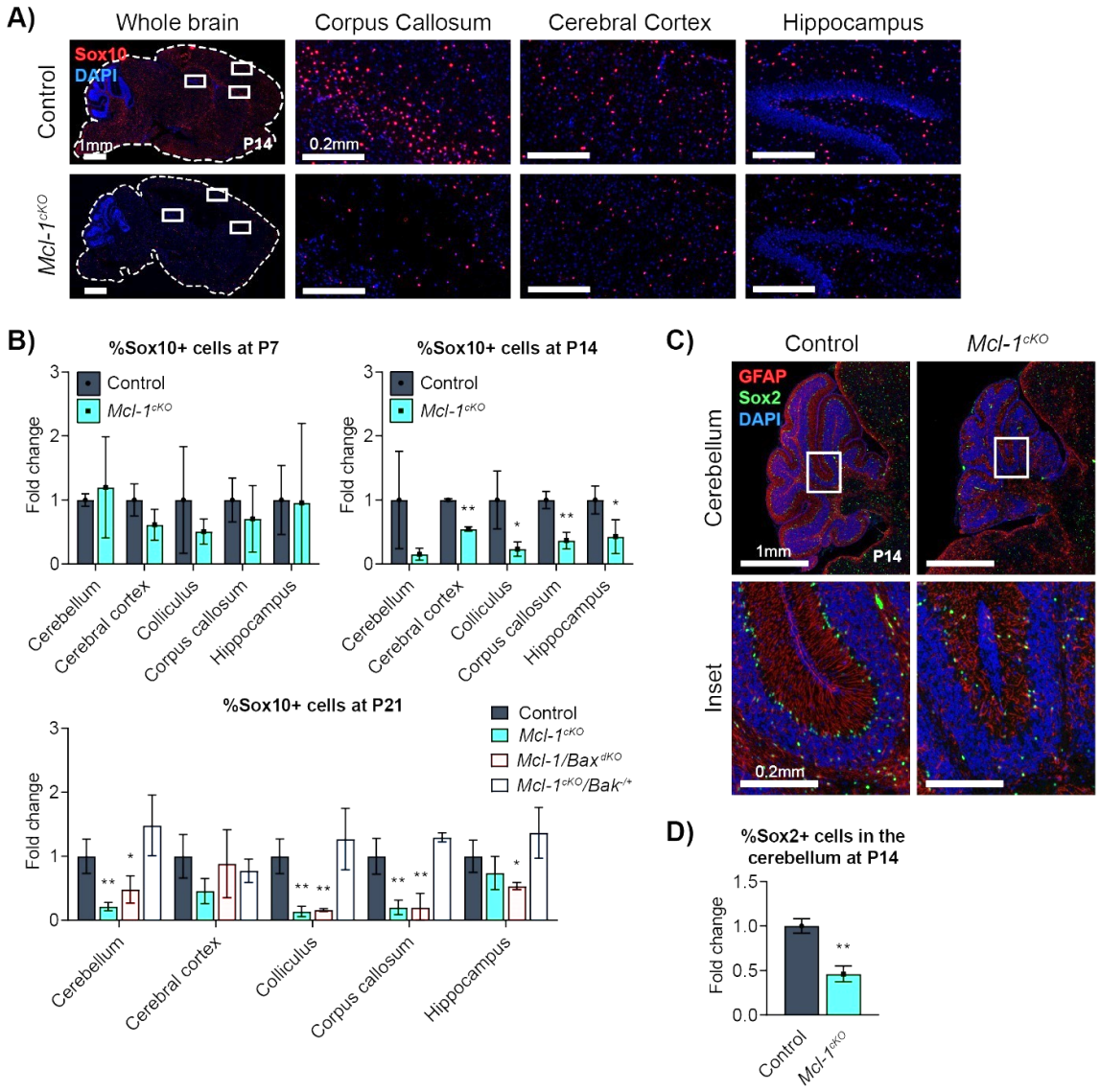

Figure 4. *Mcl-1* deletion causes loss of oligodendrocytes and Bergmann glia that is rescued with regional variation by co-deletion of *Bak* or *Bax*. (**A,B**) Representative images and quantification of SOX10 IHC in the indicated genotypes. (**C**) Representative immunofluorescence for GFAP and SOX2 IHC identify Bergmann glia in P14 mice of indicated genotypes. (**D**) SOX2+ cells are significantly reduced in *Mcl-1*^{cKO} mice. * and ** denote p<0.05 and p<0.01 respectively, relative to controls.

To determine if apoptosis mediates the decline in the oligodendrocyte populations in *Mcl-1*-deleted mice, we examined the effect of *Bax* or *Bak* co-deletion in *Mcl-1*^{cKO}*/Bak*$^{+/-}$and *Mcl-1/Bax*^{dKO} mice. Heterozygous *Bak* co-deletion in *Mcl-*

307 *1^{cKO}/Bak$^{+/-}$* mice normalized oligodendrocyte population size, but homozygous *Bax*
308 deletion in *Mcl-1/Bax^{cKO}* mice did not (Fig. 4B). *Bak* co-deletion thus rescued the
309 effects of *Mcl-1* deletion on white matter volume, myelination, and total
310 oligodendrocyte populations. In contrast, *Bax* co-deletion rescued only white matter
311 volume, but myelination and oligodendrocyte numbers remained affected in *Mcl-*
312 *1/Bax^{dKO}* mice. The discordant effects of *Bak* and *Bax* co-deletions suggest that MCL-
313 1 discretely controls BAK-dependent apoptosis or BAX-dependent apoptosis in
314 different types of white matter cells.

315 In contrast to the discordant effects of *Bax* and *Bak* co-deletions in
316 oligodendrocytes, Bergmann glia were rescued by either co-deletion. We examined
317 Bergmann glia because of their known involvement in VWMD [33], and because of the
318 migration abnormalities in *Mcl-1^{cKO}* mice, as Bergmann glia guide cerebellar granule
319 neuron progenitors as they migrate to the internal granule cell layer to become
320 cerebellar granule neurons [34,35]. We identified Bergmann glia as cells with SOX2+
321 nuclei and GFAP+ processes (Fig. 4C). At P7, the numbers of Bergmann glia in *Mcl-*
322 *1^{cKO}* were similar to control mice (data not shown), but by P14, the Bergmann glia
323 populations in *Mcl-1^{cKO}* mice were significantly reduced (Fig. 4D). The loss of
324 Bergmann glia during the period of CGN migration account for the observed
325 cerebellar migration defects. Co-deletion of either one copy of *Bak* in *Mcl-1^{cKO}/Bak$^{+/-}$*
326 mice or both copies of *Bax* in *Mcl-1/Bax^{dKO}* mice was sufficient to rescue cerebellar
327 migration, indicating that MCL-1 functions in Bergmann glia to restrict an apoptotic
328 program that requires both BAX AND BAK in order to drive cell death.

329

330

331 ***Mcl-1* deletion alters the astrocytic populations**

332 While *Mcl-1*^{cKO} mice contained fewer Bergmann glia, we noted increased
333 numbers of GFAP+ astrocytic processes throughout the brain, that was most
334 conspicuous in the relatively hypocellular molecular layer of the cerebellum (Fig. 5A).
335 To determine if this increase in GFAP+ cells indicated an increase in the total number
336 of astrocytes or an increase in the fraction of astrocytes expressing GFAP, we
337 compared the number of cells expressing the astrocytic nuclear marker SOX9 in *Mcl-*
338 *1*^{cKO} mice and controls (Fig. 5B). SOX9+ cells were not significantly increased in *Mcl-*
339 *1*^{cKO} mice in any brain region at either P7 or P14, and rather were decreased in the
340 corpus callosum at P14 (Fig. 5B,C). The increase in GFAP+ processes in *Mcl-1*^{cKO}
341 mice without the increase in SOX9+ cells shows the *Mcl-1* deletion did not increase
342 the total astrocyte population, but rather increased the fraction of astrocytes
343 expressing GFAP, indicating a reactive response to injury [36,37].

344 The intermediate filament protein NESTIN is known to be up-regulated in
345 reactive astrocytes [38-41], and prior studies report increased Nestin-expressing
346 astrocytes in white matter from humans with VWMD [42]. Similarly, *eIF2B5* $^{R191H/R191H}$
347 mice show increased astrocytes expressing both Nestin and GFAP in the corpus
348 callosum, compared to wildtype controls [20,33]. To determine if *Mcl1*-deleted mice also
349 showed similar astrocytic changes, we compared Nestin+/GFAP+ populations in P14
350 *Mcl-1*^{cKO} mice and controls (Fig. 5D). *Mcl-1*^{cKO} mice demonstrated increased fractions
351 of Nestin+/GFAP+ cells in the corpus callosum (Fig 5E), with a trend toward increased
352 fractions in other white matter regions, consistent with astrocytic changes in VWMD
353 patients and *eIF2B5* $^{R191H/R191H}$ mice. *Mcl-1*^{cKO} mice thus recapitulated both the

354 astrocytic and oligodendrocytic abnormalities seen in VWMD in patients and the
355 VWMD mouse models.

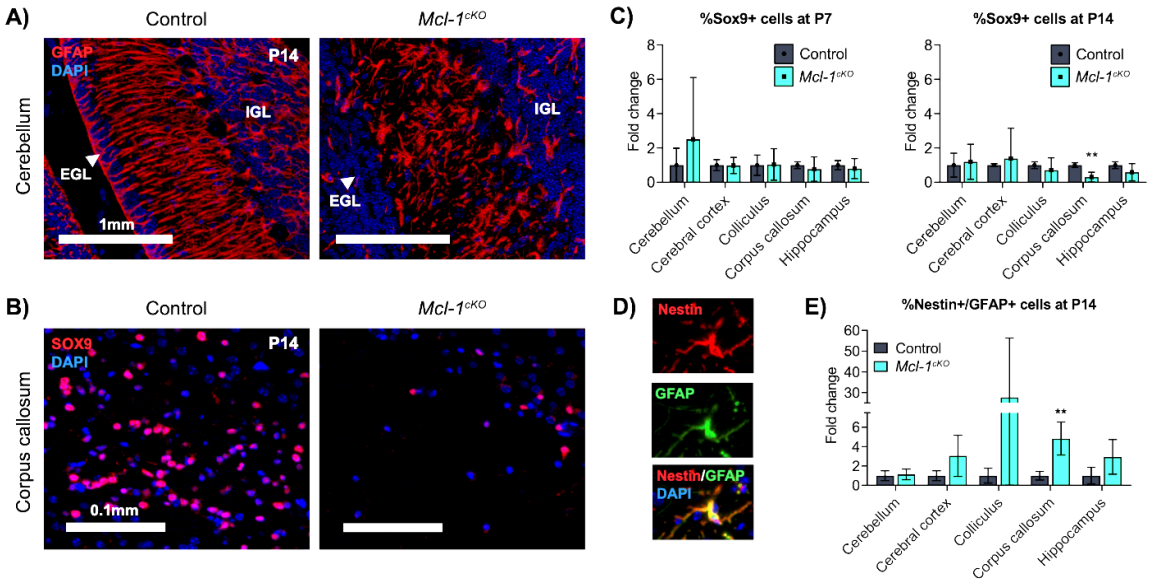

356

357 **Figure 5. Mcl-1 deletion causes reactive astrocytosis.** (**A**) Representative GFAP
358 IHC in sections of P14 cerebella in the indicated genotypes shows Bergmann glia
359 processes in the control mice that are absent in the *Mcl-1*^{cKO}, and numerous astrocyte
360 processes in the *Mcl-1*^{cKO} mice. (**B**) Representative SOX9 IHC in sections of P14
361 corpus callosum in the indicated genotypes show a significant decrease of SOX9+
362 cells in the *Mcl-1*^{cKO} mice. (**C**) Quantification of SOX9 IHC at the indicated ages and
363 genotypes, showing that astrocyte numbers are not increased in *Mcl-1*^{cKO} mice. (**D,E**)
364 Nestin/GFAP IHC, with representative images and quantification in the indicated
365 genotypes. * and ** denote $p<0.05$ and $p<0.01$ respectively, relative to controls.

366 **Mcl-1 deletion causes neuroinflammation**

367 Brains of *Mcl-1*^{cKO} mice contained increased cells expressing the myeloid
368 marker IBA1 (Fig. 6A), indicating microglial activation [43,44]. The microglial changes in
369 *Mcl-1*^{cKO} mice began later than the astrocytic and oligodendrocytic changes,
370 beginning at the corpus callosum at P14; by P21, *Mcl-1*^{cKO} mice showed increased
371 IBA+ cells in diverse brain regions (Fig. 6B). The increased IBA1+ microglia in *Mcl-*

372 *1^{cKO}* mice demonstrates a non-cell autonomous effect in which *Mcl-1* deletion in the
373 glio-neuronally restricted GFAP lineage induced inflammatory changes in myeloid
374 cells.

375 Co-deletion of either *Bak* or *Bax* prevented microgliosis in different brain
376 regions. Heterozygous co-deletion of *Bak* in *Mcl-1^{cKO}; Bak$^{+/-}$* mice significantly
377 reduced IBA1+ cells in the cerebellum, cerebral cortex, colliculus, and corpus
378 callosum, relative to *Mcl-1^{cKO}* mice. In contrast, homozygous co-deletion of *Bax* in
379 *Mcl-1$^{/}$Bax^{dKO}* mice showed a significant decrease in IBA1+ cells in the hippocampus,
380 relative to both *Mcl-1^{cKO}* and *Mcl-1^{cKO}/Bak$^{+/-}$* mice (Fig. 6B). The rescue of neuro-
381 inflammation by co-deletion of *Bax* or *Bak* implicates increased regional apoptosis as
382 the cause of inflammation, while the region-specific pattern of rescue further supports
383 the conclusion that white matter cells in different areas of the brain alternatively
384 regulate apoptosis through interactions of MCL-1 with either BAX or BAK.

385 **Decreased brain MCL-1 protein in a VWMD mouse model**

386 Based on the similarity of the *Mcl-1^{cKO}* phenotype to VWMD, the role of the ISR in
387 VWMD, and the regulation of MCL-1 abundance by the ISR, we investigated whether
388 changes in MCL-1 protein might mediate the effect of mutant eIF2B on glial cells. To
389 begin to test this possibility, we compared MCL-1 abundance in brain lysates from
390 wildtype and *eIF2B5 $^{R132H/R132H}$* mice at 7 and 10 months old (Fig. 6C). We found that
391 by 10 months, *eIF2B5 $^{R132H/R132H}$* mice expressed reduced MCL-1 protein in the brain,
392 indicating that the *eIF2B5 $^{R132H/R132H}$* mutation results in reduced MCL-1 expression
393 over time. In *eIF2B5 $^{R132H/R132H}$* mice, the temporal course of reduced brain MCL-1
394 protein correlated with the development of VWMD symptoms. Thus, along with our
395 finding that MCL-1 deficiency in *Mcl-1^{cKO}* mice was sufficient to cause a VWMD

phenotype, we found declining MCL-1 expression in *eIF2B5* $^{R132H/R132H}$ mice that model VWMD.

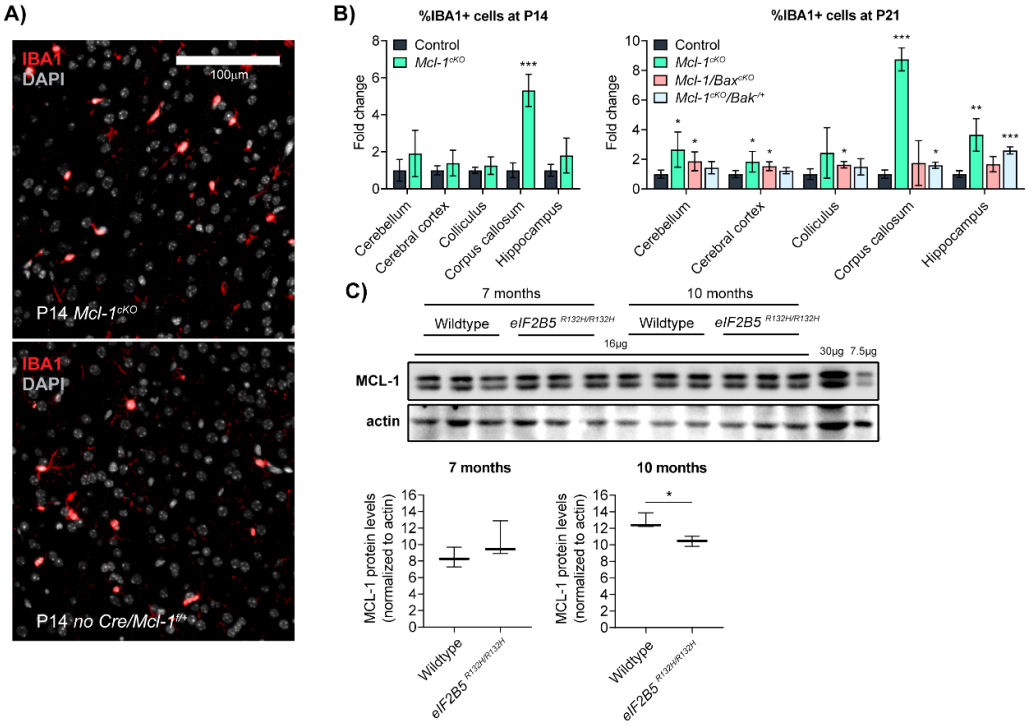

Figure 6. Progressive neuroinflammation in *Mcl-1*^{cKO} mice and reduced MCL-1 protein in mice with VWMD. (**A,B**) IBA1 IHC, with representative images and quantification in the indicated genotypes, showing a progressive increase in microglia in *Mcl-1*^{cKO} mice, beginning in the corpus callosum at P14 and expanding to include diverse regions by P21. Co-deletion of *Bak* or *Bax* variably rescue microgliosis with different effects in different regions. *, ** and *** denote $p<0.05$, $p<0.01$ and $p<0.001$ respectively, relative to controls. (**C**) Western blot comparing MCL-1 protein abundance in brain lysates of 7- and 10-months old WT and *eIF2B5*$^{R132H/R132H}$ mice, demonstrating reduced MCL-1 in 10-month old mutant mice. * denotes $p<0.03$, relative to controls.

411 **Discussion**

412 Our data show that conditional deletion of anti-apoptotic *Mcl-1* in neuro-glial
413 stem cells results in a progressive encephalopathy with post-natal white matter
414 degeneration. While MCL-1 mutations have not been described in any human
415 leukodystrophy, our data show that *Mcl-1* loss is sufficient to cause white matter
416 degeneration. The mechanisms of white matter injury in human leukodystrophies are
417 unresolved; our studies suggest that altered regulation of apoptosis, potentially
418 through disruption of MCL-1 expression, may play a central role in the pathogenesis
419 of leukodystrophies.

420 The *Mcl-1*^{cKO} phenotype presented striking similarities to human
421 leukodystrophies, and most specifically to VWMD. Brain function and white matter
422 appeared normal in *Mcl-1*^{cKO} mice until after P7, when mice showed motor and
423 sensory impairment, delayed myelination, and rarefaction of the periventricular white
424 matter and corpus callosum, eventually leading to white matter loss and
425 hydrocephalus *ex vacuo*. Similar to VWMD, mature myelinating oligodendrocytes
426 were markedly reduced, Bergmann glia of the cerebellum were also affected, and
427 astrocytes showed reactive changes that are also seen in astrocytes in VWMD,
428 including up-regulation of GFAP and NESTIN. The similarity of the *Mcl-1*^{cKO} and
429 VWMD phenotypes, including the overall histopathology of vanishing white matter
430 and the specific loss of terminally differentiated oligodendrocytes and Bergmann glia,
431 show that *eIF2B* mutations and *Mcl-1* deletion affect specific cells of the brain in a
432 similar manner.

433 Taken together, reduced MBP and SOX10 demonstrate that within global
434 oligodendrocyte depletion of *Mcl-1*^{cKO} mice, mature, myelinating oligodendrocytes are

435 particularly affected. Studies in VWMD patients and mouse models show that while
436 mature oligodendrocyte populations are reduced, immature oligodendrocyte
437 precursors may actually be increased [18,45]. A similar increase in immature
438 oligodendrocytes may occur in the *Mcl-1*^{cKO} mice and would not be inconsistent with
439 the observed overall reductions in SOX10+ brain cells and brain myelination.

440 The similarity of the *Mcl-1*^{cKO} phenotype to VWMD raises the possibility that
441 reduced MCL-1 protein abundance specifically contributes to VWMD pathology. The
442 known activation of the ISR in VWMD [16,17] and the suppression of MCL-1 translation
443 by the ISR together provide a potential molecular mechanism to link the *Mcl-1*^{cKO}
444 phenotype to VWMD. Consistent with this proposed mechanism, we found reduced
445 MCL-1 protein in *eIF2B5* $^{R132H/R132H}$ mice, which correlated with the development of
446 white matter pathology. While studies in patient-derived samples could potentially test
447 whether MCL-1 abundance is altered in VWMD patients, these studies would require
448 samples that preceded fulminant white matter loss, in order to include
449 oligodendrocyte populations that may be lost through apoptosis. Our data show that
450 MCL-1 deficiency is sufficient to reproduce the VWMD phenotype in mice. Studies of
451 *Bax* and *Bak* deletion in *eIF2B5* $^{R132H/R132H}$ mice would allow testing of whether
452 apoptosis is required for VWMD.

453 The rescue of the *Mcl-1*^{cKO} phenotype by co-deletion of *Bak* or *Bax* implicate
454 apoptosis in the causation of white matter loss in *Mcl-1*^{cKO} mice. We previously found
455 that conditional *Mcl-1* deletion in cerebellar granule neuron progenitors does not
456 produce a phenotype of gray matter loss as these cells regulate BAX via the
457 homologous anti-apoptotic protein BCL-xL [30]. The specific dependencies of different
458 cell types on different anti-apoptotic factors is also seen outside the nervous system,

459 as in the myeloid lineage where neutrophils undergo spontaneous apoptosis when
460 *Mcl-1* is deleted, but macrophages survive [23]. Different cell types within broad
461 lineages may thus require different anti-apoptotic family proteins to regulate
462 apoptosis, and the survival of neurons and astrocytes in *Mcl-1*^{cKO} mice shows that
463 within the broad lineage derived from glio-neuronal stem cells, MCL-1 protein is
464 specifically required by a subset of cells at some point along the more narrow lineage
465 of the oligodendrocytes.

466 In addition to demonstrating the requirement for apoptosis in white matter
467 degeneration in *Mcl-1*^{cKO} mice, the *Bax* and *Bak* rescue studies demonstrate that
468 myelination defects and white matter loss can be dissociated. Co-deletion of *Bak*
469 rescued both myelination, oligodendrocyte populations, and white matter loss. In
470 contrast co-deletion of *Bax* reduced white matter loss without rescuing myelination
471 and oligodendrocyte populations. These differences show that different cell types that
472 can be differentiated by their apoptosis regulation contribute to different aspects of
473 the *Mcl-1*^{cKO} phenotype.

474 The possibility that BAX and BAK act in different cells with different sensitivities
475 does not require differential expression patterns. For example, prior studies show that
476 both BAX and BAK can drive apoptosis in cerebellar granule neuron progenitors, but
477 under different conditions. BAX-dependent apoptosis in these cells can be engaged
478 either by radiation-induced DNA damage [28], or by chromosomal fragmentation in the
479 setting of *Atr* deletion [29]. In contrast, BAK-dependent apoptosis is not engaged by
480 radiation, as radiation induced apoptosis is blocked by *Bax* deletion[28,30]; BAK-
481 dependent apoptosis requires the more intense trigger of *Atr* deletion and resulting
482 chromosomal fragmentation [29]. These prior studies show that cells in the CNS that

483 express both BAX and BAK can show different mechanisms and sensitivities for
484 triggering BAX-dependent or BAK-dependent apoptosis. Similarly, specific subsets of
485 glia may regulate BAX-dependent and BAK-dependent apoptosis through different
486 mechanisms, with different, cell-type specific sensitivities and dependencies on MCL-
487 1.

488 The rescue myelination by co-deletion of *Bak* but not *Bax* shows that
489 myelinating oligodendrocytes or their precursors regulate apoptosis specifically
490 through MCL-1:BAK interactions. The different rescue pattern with *Bax* co-deletion,
491 which prevented white matter degeneration without normalizing myelination, shows
492 that a different type of cell regulates white matter loss and requires both BAK and
493 BAX to be present for *Mcl-1* deletion to produce phenotype changes. Clearly, diverse
494 cell types are affected in both *Mcl-1*^{cKO} mice and VWMD patients [9,46]. Our genetic
495 rescue studies show that different types of glial cells depend on MCL-1 to regulate
496 different pro-apoptotic proteins, and that loss of this regulation in different types of
497 cells reproduces different aspects of the overall pathology. The loss of multiple
498 subsets of glial cells may similarly contribute to different aspects of the overall VWMD
499 phenotype.

500 While multiple mutations can cause leukodystrophies, for many of these
501 genetic diseases, the mechanistic steps from mutation to white matter loss remain to
502 be specified in detail. Our findings that MCL-1 deletion in neuro-glial stem cells
503 produces white matter degeneration, and that this degeneration is rescued by co-
504 deletion of *Bax* or *Bak* implicates the process of apoptosis in the causation of
505 leukodystrophy. Moreover, our rescue experiments show that apoptosis in multiple
506 cell types derived from neuro-glial stem cells contribute to different aspects of white

507 matter pathology. Treatments that inhibit the intrinsic apoptotic pathway in the
508 postnatal brain may provide an avenue for reducing the impact of diverse
509 leukodystrophies.

510 **Methods**

511

512 **Mice**

513

514 We generated *Mcl-1*^{cKO} mice, by crossing *GFAP-Cre* mice (Jackson Labs, stock #
515 004600) with *Mcl-1*$^{LoxP/LoxP}$ mice [23], generously shared by Dr. You-Wen He. We
516 interbred GFAP-Cre, *Mcl-1*$^{loxP/loxP}$, and *Bax*$^{LoxP/LoxP}$*/Bak*$^{-/-}$ (Jackson Labs, stock #
517 006329) to generate *Mcl-1;Bax*^{dKO}, *Mcl-1;Bak*^{dKO}, and various heterozygous controls.
518 We generated *EMX1-Cre/Mcl-1*$^{loxP/loxP}$ mice by breeding *EMX1-Cre* mice, generously
519 provided by Dr. William Snide, into the *Mcl-1 f/f* line. All mice were of species *Mus*
520 *musculus* and crossed into the C57BL/6 background through at least five generations.
521 All animal studies were carried out with the approval of the University of North
522 Carolina Institutional Animal Care and Use Committee under protocols (19-099).
523 Wild type (C57BL/6 strain) and *eIF2B5*$^{R132H/R132H}$ mice [20] were generated, bred,
524 and housed in Tel Aviv University animal facility (Lab Products Inc., Seaford, DE,
525 USA). All experimental procedures were approved by the Tel Aviv University Animal
526 Care Committee according to national guidelines (permit #04-17-022). Breeding and
527 genotyping were performed as previously described. [20] Each generation was
528 established by back cross of homozygous *eIF2B5*$^{R132H/R132H}$ mice with WT C57BL/6J
529 (Harlan Labs, Jerusalem, Israel) to prevent genetic drift.

530

531 **Histology and immunohistochemistry (IHC)**

532

533 Mouse brains were processed and immunostained as previously described [29,47-49].
534 Primary antibodies used were: BAK diluted 1:200 (Cell Signaling, #12105), MBP
535 diluted 1:1000 (Abcam, #ab7349), SOX10 diluted 1:100 (Santa Cruz, #sc-17342),
536 cleaved-Caspase 3 (cC3) diluted 1:400 (Biocare Medical, #CP229C), glial fibrillary
537 acidic protein (GFAP) diluted 1:2000 (Dako, Z0334), SOX2 1:200 (Cell Signaling,
538 #4900S), SOX9 1:200 (R&D Systems, #AF3075), NESTIN 1:500 (Cell Signaling,
539 #4760), IBA1 1:2000 (Wako Chemicals, #019-19741). Stained images were
540 counterstained with DAPI, digitally imaged using an Aperio Scan Scope XT (Aperio)
541 and subjected to automated cell counting using Tissue Studio (Definiens).

542

543 **Magnetic resonance imaging**

544

545 For MRI studies, brains from P7, P14, and P21 mice were harvested and fixed in 4%
546 formaldehyde in PBS for 48hrs, then transferred to PBS. Brains were then embedded
547 in 2% agarose in 15mL plastic vials and imaged in pairs as previously described
548 (Williams et al., 2015).

549

550 **Western blot**

551

552 Whole brains or cerebella were harvested and homogenized in lysis buffer (Cell
553 Signaling, #9803). Lysate protein concentrations were quantified using a
554 bicinchoninic acid (BCA) protein assay kit (Thermo scientific, #23225). Equal total
555 protein concentrations were resolved on SDS-polyacrylamide gels (BioRad, #
556 4561105, # 4568094) and transferred onto polyvinylidene difluoride membranes.

557 Membranes were blotted using a SNAP i.d. 2.0 Protein Detection System (Millipore).
558 Membranes were imaged using a chemiluminescent SuperSignal West Femto
559 Maximum Sensitivity Substrate (34095, Thermo Fisher Scientific) and the C-DiGit blot
560 scanner (LI-COR Biosciences). Signal was quantified using the Image Studio Lite
561 software (LI-COR). The following antibodies were used for western blot: MCL-1 (Cell
562 Signaling, #94296; 1:500 dilution), BAX (Cell Signaling, #14796; 1:500 dilution), β-
563 actin (Cell Signaling, #3700; 1:5000 dilution), Actin (Sigma #A3853; 1:240000
564 dilution), Anti-rabbit IgG, HRP-linked antibody (Cell Signaling, #7074; 1.5:1000
565 dilution), Anti-mouse IgG, HRP-linked antibody (Cell Signaling, #7076; 1.5:1000
566 dilution). For the eIF2B5$^{R132H/R132H}$ studies, cerebrums were harvested from 7 and 10
567 month old mice and protein was extracted using a lysis buffer containing 1% triton,
568 0.5% NaDOC, 0.1% SDS, 50 mM Tris pH 8, 100 mM NaCl, 10 mM β-
569 glycerophosphate, 5 mM NaF, 1 mM DTT, 1 mM vanadate, and EDTA-free complete
570 TM protease inhibitor cocktail (#11-836-170-001; ROCHE). Protein was quantified
571 using a BCA protein assay kit (#23227 Pierce), diluted in 1X sample buffer (0.05 M
572 HEPES pH 7.4, 2% (w/v) SDS, 10% (v/v) Glycerol, traces of Bromophenol Blue, 100
573 mM Dithiothreitol (DTT)), and separated on a 10% SDS-PAGE gel. Blots were imaged
574 using an AI600 Imager (Amersham) and quantified by ImageQuant TL (GE
575 Healthcare, Pittsburgh, PA, United States).
576
577 **Behavioral studies**
578
579 **Animals included.** Subjects were *Mcl-1^{cKO}* mice or littermate controls with intact Mcl-
580 1, including genotypes Mcl1$^{f/+}$ without Cre, Mcl1$^{f/f}$ without Cre, and Gfap-Cre/Mcl1$^{f/+}$.
581 A total of 8 litters were needed to generate all of the replicates. Day of birth was

582 considered postnatal day 0 (P0). Subject numbers at the beginning of the study (P7)
583 were 13 (21%) *Mcl-1*^{cKO} and 48 (79%) control. All litters completed the first 2 weeks
584 of testing. Three litters (n=23) were removed from the study for histology assays
585 during the third week of testing: one on P15, after the second open field test; one on
586 PD16, after the first acoustic startle test; and one on P21, after the tail suspension
587 test.
588
589 **Behavioral testing regimen**
590
591 **Developmentally-calibrated behavioral tests:** For motor tests at P7, mice were
592 removed from the home cage and maintained in a beaker warmed to 35°C. Mice were
593 then subjected to the neurobehavioral negative geotaxis, righting, and open field
594 tests, adapted from published studies [50].
595 **Negative geotaxis**. A 20 cm × 20 cm screen with 0.5 cm wire mesh squares was set
596 at a 25° angle. Each pup was placed downward on the screen with its head facing
597 toward the bottom, allowed to grip the mesh, and then released. The time it took for
598 each pup to turn 180° (head and upper torso vertical), was recorded, with a 30 s
599 maximum and each pup was tested 3 times.
600 **Righting.** Each pup was placed onto its back on a flat Plexiglas surface. The
601 experimenter gently held the pup in place for 2 s and then released it. The latency to
602 righting (all 4 feet on the ground) was timed, with a maximum of 30 s.
603 **Open field activity and pivoting.** Each pup was placed into the center of a Plexiglas
604 chamber (PhenoTyper; 30.5 cm × 30.5 cm × 43.5 cm; Noldus Information
605 Technology, Wageningen, The Netherlands). A dim yellow light (30 lx) at the top of
606 the PhenoTyper box was illuminated throughout the 3 min trial. Measures were taken

607 of distance traveled and time in the center region (4 cm × 4 cm square in the center
608 of the arena) by an image-tracking system (EthoVision, Noldus Information
609 Technology). In addition, the experimenter recorded the number of vertical rearing
610 movements and number of pivots (circling or lateral movement, as opposed to
611 forward locomotion).

612 Each mouse was screened through the 3 assays in the order presented here. After
613 finishing the neonatal motor screen, each pup was weighed, marked with a non-toxic
614 Sharpie, and placed back into the warm beaker. The litter was returned to the home
615 cage after all pups had been tested.

616

617 **Open field activity at P14 and P19.** Additional open field activity tests were
618 performed at P14 and P19. The distance traveled, the number of vertical rearing
619 movements, and time spent in the center region was recorded in each 10 min test.

620

621 **Acoustic startle responses.** This test was used to assess auditory function,
622 reactivity to environmental stimuli, and sensorimotor gating. Mice were evaluated at
623 2 time points, P14 and P21. The procedure was based on the reflexive whole-body
624 flinch, or startle response, that follows exposure to the acoustic stimuli. Measures
625 were taken of startle magnitude and prepulse inhibition, which occurs when a weak
626 stimulus leads to a reduced startle in response to a subsequent louder noise.

627 Mice were placed into individual Plexiglas cylinders within larger, sound-
628 attenuating chambers. Each cylinder was seated upon a piezoelectric transducer,
629 which allowed vibrations to be quantified and displayed on a computer (San Diego
630 Instruments SR-Lab system). The chambers included a ceiling light, fan, and a
631 loudspeaker for the acoustic stimuli. Background sound levels (70 dB) and calibration

632 of the acoustic stimuli were confirmed with a digital sound level meter (San Diego
633 Instruments). Each session began with a 5-min habituation period, followed by 42
634 trials of 7 different types: no-stimulus (NoS) trials, trials with the acoustic startle
635 stimulus (AS; 40 msec, 120 dB) alone, and trials in which a prepulse stimulus (20
636 msec; either 74, 78, 82, 86, or 90 dB) occurred 100 ms before the onset of the startle
637 stimulus. Measures were taken of the startle amplitude for each trial across a 65-
638 msec sampling window, and an overall analysis was performed for each subject's
639 data for levels of prepulse inhibition at each prepulse sound level (calculated as 100
640 - [(response amplitude for prepulse stimulus and startle stimulus together / response
641 amplitude for startle stimulus alone) x 100].
642
643 **Limb clasping.** At PD18-21, a subset of mice (n=39) was assessed for limb clasping
644 during a tail-suspension test. Each mouse was lifted by the base of the tail, and
645 suspended above cage bedding for 15 sec, with ventral (stomach) side facing the
646 experimenter. Response to tail suspension was coded using the following scoring
647 system:
648
649 Forepaw movement
650 -2 = paws are clasped together, little movement, may be drawn up against
651 chest
652 0 = paws move quickly in periodic flailing or kicking motions
653 2 = vigorous movement, may resemble rapid digging
654 Hindlimb placement and movement
655 -4 = both hindlimbs are retracted inwards toward abdomen, with little
656 movement

657 -2 = hindlimbs are partially or intermittently retracted inwards toward abdomen

658 0 = hindlimbs are splayed outward from the abdomen. Moderate kicking behavior

659 2 = vigorous rapid kicking

660

661 **Statistical analysis of behavioral tests**

662

663 All testing was conducted by experimenters blinded to mouse genotype. Statview

664 (SAS, Cary, NC) was used for data analyses. To reduce the number of *Mcl-1*^{cKO}

665 subjects required, behavioral data from males and females were combined. One-

666 way or repeated measures analysis of variance (ANOVA) were used to determine

667 effects of genotype. Post-hoc analyses were conducted using Fisher's Protected

668 Least Significant Difference (PLSD) tests following a significant ANOVA F value. For

669 all comparisons, significance was set at $p<0.05$.

670

671

672 **Supplementary Figures**

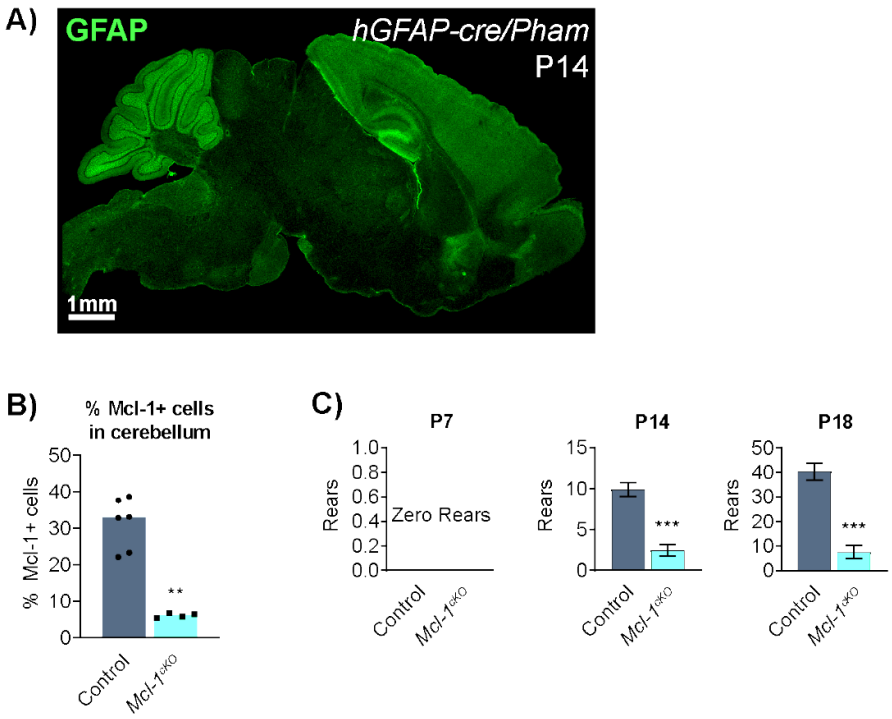

673

674 **Supplementary Figure 1. *hGFAP-Cre* conditionally deletes *Mcl-1* in regions**
675 **throughout the brain. A)** *hGFAP-Cre* induces expression of the fluorescent reporter
676 DENDRA2 in *hGFAP-cre/Pham* mice, indicating regions of GFAP expression. *hGFAP-*
677 *Cre* targets cells in diverse regions throughout the brain, including the cerebellum,
678 hippocampus, and cortex. **B)** MCL-1 protein levels are significantly reduced in
679 cerebella of *Mcl-1*^{cKO} mice. **C)** *Mcl-1*^{cKO} mice displayed decreased rearing at both P14
680 and P18.

681

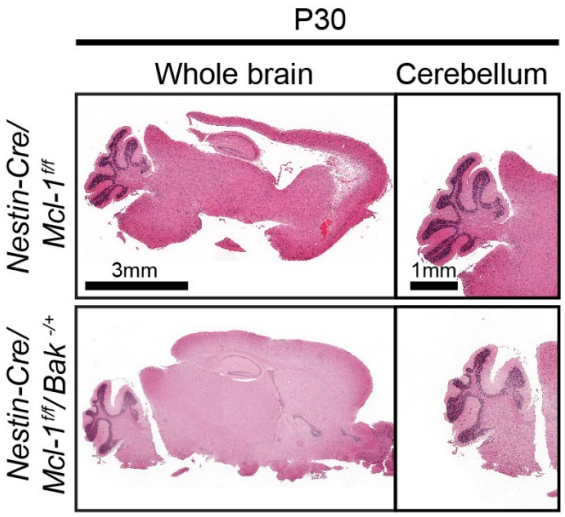

682

683 **Supplementary Figure 2. *Nestin-Cre/Mcl-1$^{f/f}$* mice develop white matter**
684 **degeneration similar to that of *Mcl-1^{cKO}* mice.** Similar to GFAP-Cre, Nestin-Cre
685 targets cells of both the neural and glial lineage. Brains harvested from *Nestin-*
686 *Cre/Mcl-1$^{f/f}$* mice showed ventricular dilation and white matter rarefaction by P30.
687 Deletion of one copy of *Bak* rescued this phenotype in *Nestin-Cre/Mcl-1$^{f/f}$/Bak$^{-/+}$* mice.

688

689

690 **References**

691

692 1 Raymond, G. V. Leukodystrophy: Basic and Clinical. *Adv Neurobiol* **15**, 365-382,
693 doi:10.1007/978-3-319-57193-5_14 (2017).
694 2 van der Knaap, M. S. & Bugiani, M. Leukodystrophies: a proposed classification
695 system based on pathological changes and pathogenetic mechanisms. *Acta*
696 *Neuropathol* **134**, 351-382, doi:10.1007/s00401-017-1739-1 (2017).
697 3 Kohler, W., Curiel, J. & Vanderver, A. Adulthood leukodystrophies. *Nat Rev Neurol*
698 **14**, 94-105, doi:10.1038/nrneurol.2017.175 (2018).
699 4 Kohlschutter, A. & Eichler, F. Childhood leukodystrophies: a clinical perspective.
700 *Expert Rev Neurother* **11**, 1485-1496, doi:10.1586/ern.11.135 (2011).
701 5 Vanderver, A., Tonduti, D., Schiffmann, R., Schmidt, J. & van der Knaap, M. S. in
702 *GeneReviews((R))* (eds M. P. Adam *et al.*) (1993).
703 6 van der Knaap, M. S. & Bugiani, M. Leukodystrophies - much more than just diseases
704 of myelin. *Nat Rev Neurol* **14**, 747-748, doi:10.1038/s41582-018-0093-9 (2018).
705 7 Melchionda, L. *et al.* Mutations in APOPT1, encoding a mitochondrial protein, cause
706 cavitating leukoencephalopathy with cytochrome c oxidase deficiency. *Am J Hum*
707 *Genet* **95**, 315-325, doi:10.1016/j.ajhg.2014.08.003 (2014).
708 8 Yasuda, O. *et al.* Apop-1, a novel protein inducing cyclophilin D-dependent but
709 Bax/Bak-related channel-independent apoptosis. *J Biol Chem* **281**, 23899-23907,
710 doi:10.1074/jbc.M512610200 (2006).
711 9 Bugiani, M., Vuong, C., Breur, M. & van der Knaap, M. S. Vanishing white matter: a
712 leukodystrophy due to astrocytic dysfunction. *Brain Pathol* **28**, 408-421,
713 doi:10.1111/bpa.12606 (2018).
714 10 van der Knaap, M. S. *et al.* A new leukoencephalopathy with vanishing white matter.
715 *Neurology* **48**, 845-855, doi:10.1212/wnl.48.4.845 (1997).
716 11 van der Knaap, M. S., Fogli, A., Boespflug-Tanguy, O., Abbink, T. E. M. & Schiffmann,
717 R. in *GeneReviews((R))* (eds M. P. Adam *et al.*) (1993).
718 12 van der Knaap, M. S., Pronk, J. C. & Scheper, G. C. Vanishing white matter disease.
719 *Lancet Neurol* **5**, 413-423, doi:10.1016/S1474-4422(06)70440-9 (2006).
720 13 Fogli, A. *et al.* Cree leukoencephalopathy and CACH/VWM disease are allelic at the
721 EIF2B5 locus. *Ann Neurol* **52**, 506-510, doi:10.1002/ana.10339 (2002).
722 14 Leegwater, P. A. *et al.* Subunits of the translation initiation factor eIF2B are mutant in
723 leukoencephalopathy with vanishing white matter. *Nat Genet* **29**, 383-388,
724 doi:10.1038/ng764 (2001).
725 15 Bugiani, M., Boor, I., Powers, J. M., Scheper, G. C. & van der Knaap, M. S.
726 Leukoencephalopathy with vanishing white matter: a review. *J Neuropathol Exp*
727 *Neurol* **69**, 987-996, doi:10.1097/NEN.0b013e3181f2eafa (2010).
728 16 Abbink, T. E. M. *et al.* Vanishing white matter: deregulated integrated stress
729 response as therapy target. *Ann Clin Transl Neurol* **6**, 1407-1422,
730 doi:10.1002/acn3.50826 (2019).
731 17 Kantor, L. *et al.* Heightened stress response in primary fibroblasts expressing mutant
732 eIF2B genes from CACH/VWM leukodystrophy patients. *Hum Genet* **118**, 99-106,
733 doi:10.1007/s00439-005-0024-x (2005).

734 18 Herrero, M., Mandelboum, S. & Elroy-Stein, O. eIF2B Mutations Cause Mitochondrial
735 Malfunction in Oligodendrocytes. *Neuromolecular Med* **21**, 303-313,
736 doi:10.1007/s12017-019-08551-9 (2019).
737 19 Raini, G. *et al.* Mutant eIF2B leads to impaired mitochondrial oxidative
738 phosphorylation in vanishing white matter disease. *J Neurochem* **141**, 694-707,
739 doi:10.1111/jnc.14024 (2017).
740 20 Geva, M. *et al.* A mouse model for eukaryotic translation initiation factor 2B-
741 leucodystrophy reveals abnormal development of brain white matter. *Brain* **133**,
742 2448-2461, doi:10.1093/brain/awq180 (2010).
743 21 Elroy-Stein, O. Mitochondrial malfunction in vanishing white matter disease: a
744 disease of the cytosolic translation machinery. *Neural Regen Res* **12**, 1610-1612,
745 doi:10.4103/1673-5374.217329 (2017).
746 22 Fritsch, R. M., Schneider, G., Saur, D., Scheibel, M. & Schmid, R. M. Translational
747 repression of MCL-1 couples stress-induced eIF2 alpha phosphorylation to
748 mitochondrial apoptosis initiation. *J Biol Chem* **282**, 22551-22562,
749 doi:10.1074/jbc.M702673200 (2007).
750 23 Dzhagalov, I., St John, A. & He, Y. W. The antiapoptotic protein Mcl-1 is essential for
751 the survival of neutrophils but not macrophages. *Blood* **109**, 1620-1626,
752 doi:10.1182/blood-2006-03-013771 (2007).
753 24 Zhuo, L. *et al.* hGFAP-cre transgenic mice for manipulation of glial and neuronal
754 function in vivo. *Genesis* **31**, 85-94 (2001).
755 25 Kuang, Y. *et al.* Dicer1 and MiR-9 are required for proper Notch1 signaling and the
756 Bergmann glial phenotype in the developing mouse cerebellum. *Glia* **60**, 1734-1746,
757 doi:10.1002/glia.22392 (2012).
758 26 Guyenet, S. J. *et al.* A simple composite phenotype scoring system for evaluating
759 mouse models of cerebellar ataxia. *J Vis Exp*, doi:10.3791/1787 (2010).
760 27 Nakamura, A. *et al.* Bcl-xL Is Essential for the Survival and Function of Differentiated
761 Neurons in the Cortex That Control Complex Behaviors. *J Neurosci* **36**, 5448-5461,
762 doi:10.1523/JNEUROSCI.4247-15.2016 (2016).
763 28 Chong, M. J. *et al.* Atm and Bax cooperate in ionizing radiation-induced apoptosis in
764 the central nervous system. *Proceedings of the National Academy of Sciences* **97**,
765 889-894, doi:10.1073/pnas.97.2.889 (2000).
766 29 Lang, P. Y. *et al.* ATR maintains chromosomal integrity during postnatal cerebellar
767 neurogenesis and is required for medulloblastoma formation. *Development* **143**,
768 4038-4052, doi:10.1242/dev.139022 (2016).
769 30 Crowther, A. J. *et al.* Tonic activation of Bax primes neural progenitors for rapid
770 apoptosis through a mechanism preserved in medulloblastoma. *The Journal of*
771 *neuroscience : the official journal of the Society for Neuroscience* **33**, 18098-18108,
772 doi:10.1523/JNEUROSCI.2602-13.2013 (2013).
773 31 Glasgow, S. M. *et al.* Mutual antagonism between Sox10 and NFIA regulates
774 diversification of glial lineages and glioma subtypes. *Nat Neurosci* **17**, 1322-1329,
775 doi:10.1038/nn.3790 (2014).
776 32 Nishiyama, A., Boshans, L., Goncalves, C. M., Wegrzyn, J. & Patel, K. D. Lineage, fate,
777 and fate potential of NG2-glia. *Brain Res* **1638**, 116-128,
778 doi:10.1016/j.brainres.2015.08.013 (2016).
779 33 Dooves, S. *et al.* Astrocytes are central in the pathomechanisms of vanishing white
780 matter. *J Clin Invest* **126**, 1512-1524, doi:10.1172/JCI83908 (2016).

781 34 Hatten, M. E. Riding the glial monorail: a common mechanism for glial-guided
782 neuronal migration in different regions of the developing mammalian brain. *Trends*
783 *Neurosci* **13**, 179-184, doi:10.1016/0166-2236(90)90044-b (1990).
784 35 Rakic, P. Neuron-glia relationship during granule cell migration in developing
785 cerebellar cortex. A Golgi and electronmicroscopic study in Macacus Rhesus. *J Comp*
786 *Neurol* **141**, 283-312, doi:10.1002/cne.901410303 (1971).
787 36 Eddleston, M. & Mucke, L. Molecular profile of reactive astrocytes--implications for
788 their role in neurologic disease. *Neuroscience* **54**, 15-36, doi:10.1016/0306-
789 4522(93)90380-x (1993).
790 37 Dahl, D. & Bignami, A. Heterogeneity of the glial fibrillary acidic protein in gliosed
791 human brains. *J Neurol Sci* **23**, 551-563, doi:10.1016/0022-510x(74)90027-6 (1974).
792 38 Tamagno, I. & Schiffer, D. Nestin expression in reactive astrocytes of human
793 pathology. *J Neurooncol* **80**, 227-233, doi:10.1007/s11060-006-9181-6 (2006).
794 39 Schmidt-Kastner, R. *et al.* Astrocytes react to oligemia in the forebrain induced by
795 chronic bilateral common carotid artery occlusion in rats. *Brain Res* **1052**, 28-39,
796 doi:10.1016/j.brainres.2005.06.018 (2005).
797 40 Sahin Kaya, S., Mahmood, A., Li, Y., Yavuz, E. & Chopp, M. Expression of nestin after
798 traumatic brain injury in rat brain. *Brain Res* **840**, 153-157, doi:10.1016/s0006-
799 8993(99)01757-6 (1999).
800 41 Clarke, S. R., Shetty, A. K., Bradley, J. L. & Turner, D. A. Reactive astrocytes express
801 the embryonic intermediate neurofilament nestin. *Neuroreport* **5**, 1885-1888,
802 doi:10.1097/00001756-199410000-00011 (1994).
803 42 Bugiani, M. *et al.* Defective glial maturation in vanishing white matter disease. *J*
804 *Neuropathol Exp Neurol* **70**, 69-82, doi:10.1097/NEN.0b013e318203ae74 (2011).
805 43 Ito, D. *et al.* Microglia-specific localisation of a novel calcium binding protein, Iba1.
806 *Brain Res Mol Brain Res* **57**, 1-9, doi:10.1016/s0169-328x(98)00040-0 (1998).
807 44 Imai, Y., Ibata, I., Ito, D., Ohsawa, K. & Kohsaka, S. A novel gene iba1 in the major
808 histocompatibility complex class III region encoding an EF hand protein expressed in
809 a monocytic lineage. *Biochem Biophys Res Commun* **224**, 855-862,
810 doi:10.1006/bbrc.1996.1112 (1996).
811 45 Bugiani, M. *et al.* Hyaluronan accumulation and arrested oligodendrocyte progenitor
812 maturation in vanishing white matter disease. *Brain* **136**, 209-222,
813 doi:10.1093/brain/aws320 (2013).
814 46 Zhou, L. *et al.* Modeling vanishing white matter disease with patient-derived induced
815 pluripotent stem cells reveals astrocytic dysfunction. *CNS Neurosci Ther* **25**, 759-771,
816 doi:10.1111/cns.13107 (2019).
817 47 Ocasio, J. K., Bates, R. D. P., Rapp, C. D. & Gershon, T. R. GSK-3 modulates SHH-driven
818 proliferation in postnatal cerebellar neurogenesis and medulloblastoma.
819 *Development* **146**, doi:10.1242/dev.177550 (2019).
820 48 Tech, K. *et al.* Pyruvate Kinase Inhibits Proliferation during Postnatal Cerebellar
821 Neurogenesis and Suppresses Medulloblastoma Formation. *Cancer Res* **77**, 3217-
822 3230, doi:10.1158/0008-5472.CAN-16-3304 (2017).
823 49 Crowther, A. J. *et al.* Radiation Sensitivity in a Preclinical Mouse Model of
824 Medulloblastoma Relies on the Function of the Intrinsic Apoptotic Pathway. *Cancer*
825 *Res* **76**, 3211-3223, doi:10.1158/0008-5472.CAN-15-0025 (2016).

50 Cheh, M. A. *et al.* En2 knockout mice display neurobehavioral and neurochemical alterations relevant to autism spectrum disorder. *Brain Res* **1116**, 166-176, doi:10.1016/j.brainres.2006.07.086 (2006).